Chaotic saddles in a gravitational field: The case of inertial particles in finite domains

Gábor Drótos and Tamás Tél

Institute for Theoretical Physics, Eötvös University, Pázmány Péter sétány 1/A, Budapest, H-1117, Hungary

The motion of inertial particles is investigated numerically in a time-periodic flow in the presence of gravity. The flow is restricted to a finite (or semi-infinite) vertical column, and the dynamics is therefore transiently chaotic. The long-term motion of the center of mass is a uniform settling. The settling velocity is found to differ from the one that would characterize a still fluid, and the distribution of an ensemble of settling particles spreads with a well-defined diffusion coefficient. The underlying chaotic saddle appears to have a height-dependent fractal dimension. The coarse-grained density of both the natural measure and the conditionally invariant measure (defined along the unstable manifold) of the saddle is smooth, and exhibits a local maximum as a function of the height. The latter density corresponds to the eigenfunction of the first eigenvalue of an effective Fokker–Planck equation subject to an absorbing boundary condition at the bottom. The transport coefficients can be determined as averages taken with respect to the conditionally invariant measure.

I. INTRODUCTION

The dynamics of inertial particles [1–6] in fluid flows have been studied intensively in the last decade (for a review see [7,8]), and it has been shown to have important effects in many situations of practical interest ranging from atmospheric sciences [9–12] to oceanography [13–15].

As a particular case, the dynamics of particles that are heavier than the surrounding fluid came more and more into focus in the last years. This increasing recent interest stems from the fact that droplets and heavy particles play an important role in some environmental problems and industrial applications. For instance, droplet dynamics form an essential part of the complex phenomena taking place in clouds [16,17]. The sedimentation of volcanic ash is a basic component of the hazard due to volcanic eruptions [18]. On the other hand, droplets are responsible for interesting phenomena observed recently in a probably less known industrial application, for example, in demixing experiments of binary fluids [19–21].

Our aim is to investigate numerically the dynamics of sedimenting particles in a flow model that extends over a finite region, below and above which another type of hydrodynamical behavior follows. This particular choice can mimic the fact that the motion of water droplets is different within and outside the cloud, and that of volcanic ash particles is different in the free atmosphere and in the planetary boundary layer. In demixing experiments the two phases of the binary fluid are separated by a horizontal meniscus, and droplets nucleated in the upper phase will sediment and escape to the lower phase.

In such situations two important factors influence the particles' motion, namely the gravitational force and the viscous drag exerted by the background flow on the particle. The dimensionless parameter characterizing the dynamics of inertial, small, spherical particles of radius a subject to Stokes drag in a fluid of kinematic viscosity ν, of typical velocity U and of linear size L is

$$A = \frac{9\rho_f \nu L}{2a^2 \rho_p U}, \tag{1}$$

the relaxation rate to the fluid velocity (the reciprocal of the so-called Stokes number, multiplied by the density ratio). Considering a cloud, for a rain droplet of radius 1 mm, in a range of $L \sim 100$ m of a large-scale flow with typical velocity of the order of $U \sim 1$ m/s, and with the density ratio of water to air $\rho_p/\rho_f \approx 10^3$, the numerical value of parameter A turns out to be of order unity, indicating that the effect of the viscous drag is important for the particle dynamics. Similar A values are obtained for larger volcanic ash particles. For cloud droplets of radius 10^{-3} mm (and for small ash particles) we obtain $A \sim 10^6$. Similarly, in the demixing experiments ($a \sim 10^{-2}$ mm, $L \sim 10^{-4}$ m, $U \sim 10^{-5}$ m/s, $\rho_p \approx \rho_f \approx 1$ g/cm^3, and $\nu \sim 10^{-6}$ m^2/s) A is of the order of 10^6. In these latter cases the limit $A \to \infty$ can be taken, which simplifies the equations of motion. Throughout the paper we investigate the richer dynamics described by a parameter A of order unity.

Apart from these two main factors, we keep our model as simple as possible. We assume that the velocity field **u** of the flow is two dimensional and is defined in the vertical plane. Particles are considered to be heavy with a density ρ_p much larger than that of the fluid $\rho_f \ll \rho_p$. The particle ensemble is assumed to be dilute so that the probability of collisions is negligible.

Thus our simplified model is not aimed to describe these complex phenomena in full complexity, rather to concentrate on dynamical systems aspects. For merely illustrative purposes we shall formulate the model as a "model cloud" but emphasize its applicability to other phenomena as well. From the point of view of dynamical systems, our main interest is on how the finite vertical extension of the flow leads to transient chaos [22] in the advection dynamics. The problem of large spatial extension has already been treated in the context of chaotic transport [23–25] with a constant prescribed drift. Here, in a hydrodynamical context, we shall also be able to investigate how a constant drift sets in due to gravity and viscous drag, and why the constant settling velocity in the presence of a flow differs from that in a medium at rest.

The paper is organized as follows. The model is introduced in the next section. Then Sec. III is devoted to the presentation and interpretation of the numerical results. We show that the
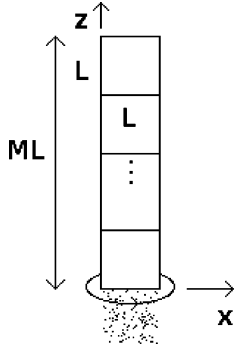
FIG. 1. Schematic diagram of the "cloud" model. In the dimensionless version of the model L is formally unity.

long term average is a uniform settling, but the settling velocity differs from the one that would characterize a still fluid, and the distribution of an ensemble of settling particles spreads with a well-defined diffusion coefficient. The underlying chaotic saddle appears to have a height-dependent fractal dimension. The coarse-grained density of both the natural measure and the conditionally invariant measure of the saddle is smooth, and exhibits a local maximum as a function of the height. In Sec. IV we show that in a semi-infinite column the latter density can be well approximated by the eigenfunction of the first eigenvalue of an effective Fokker–Planck equation subject to an absorbing boundary condition at the bottom. The results imply that a difference in the settling velocity in the moving and in the resting media is due to the conditionally invariant measure. In the concluding Sec. V we discuss our findings.

II. THE MODEL

The equations of motion for small, inertial, spherical particles in a viscous fluid are given by the Maxey-Riley equations [26,27]. For heavy particles the dimensionless Maxey-Riley equations simplify to

$$\ddot{\mathbf{r}} = A[\mathbf{u}(\mathbf{r},t) - \dot{\mathbf{r}} - W\mathbf{n}], \tag{2}$$

where $\mathbf{u}(\mathbf{r},t)$ is the flow field, W is the dimensionless terminal fall velocity, also called the settling velocity, in still fluid, and $\mathbf{n}$ is a unit vector pointing upward. Throughout the paper we fix the dimensionless relaxation rate to be $A = 5$, and the dimensionless settling velocity W to be of the order of 0.1.

We consider z to be the vertical coordinate and the flow is assumed to be translation invariant in direction y. The model flow consists of elementary cells of linear size L which are repeated periodically in the horizontal x direction. Vertically, however, the flow contains a finite number M of cells only. The model cloud can thus be represented by a vertical column of M cells subject to a periodic boundary condition in the horizontal direction (as illustrated by Fig. 1). Advection dynamics (2) is followed within this column only, after leaving the lower or the upper edge (at $z = 0$ or $z = M$), particles are considered as escaped.

The flow within a cell is taken to be a paradigmatic mixing model, the double shear flow [28,29]. The flow is periodic with temporal period L/U (i.e., with unit period in the dimensionless version) and consists of sinusoidal shears. We consider a temporally smoothened version [3,6] of the model where the change in the flow direction is continuous in time as described by the velocity components

$$u_x(\mathbf{r},t) = B\{1 + \tanh[\gamma \sin(2\pi t)]\} \sin(2\pi z),$$
$$u_z(\mathbf{r},t) = B\{1 - \tanh[\gamma \sin(2\pi t)]\} \sin(2\pi x). \tag{3}$$

Here γ is a switching parameter whose value is taken to be $\gamma = 20/\pi$, and the dimensionless flow amplitude is chosen as $B = 0.5$.

III. RESULTS

A. Long-term settling

First, we are interested in the long-term behavior of an ensemble of particles in a long column. We consider a column of height $M = 100$ and uniformly fill a single cell ($79 < z < 80$) with particles at rest, of number $N \gg 1$, as initial condition. By numerically monitoring the dynamics (2) of this ensemble of particles, we create for each time step the histogram of the z coordinates and also determine their average $Z(t)$ (the center of mass) and variance $\sigma(t)$. The settling velocity W is chosen to be $W = 0.2$.

By about $t = 10$ a "steady" behavior is developed. The motion of the center of mass is a uniform settling: $Z(t) = -wt + Z_0$, with $w = 0.28$ and $Z_0 = 79.7$. It is remarkable that velocity w strongly differs from $W = 0.2$, the settling velocity in still fluid. The variance clearly exhibits a diffusional behavior of the form of $\sigma(t)^2 = 2Dt + \sigma_0^2$, with diffusion coefficient $D = 0.03$ and with $\sigma_0^2 = 0.3$. In Fig. 2 we can see
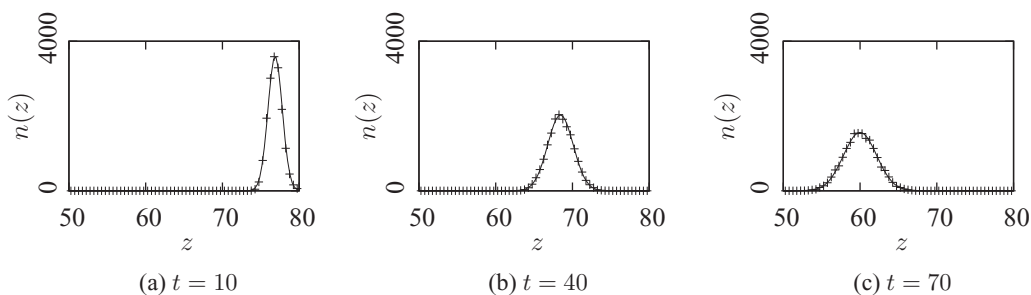

(a) $t = 10$ (b) $t = 40$ (c) $t = 70$

FIG. 2. Dynamics of an ensemble of particles in a long column along the z direction as represented by the histogram of their z coordinates. The initial uniform distribution concentrated in a single cell (cell 80) is smeared out in the Gaussian form (4) (continuous line). $W = 0.2$, $N \approx 1.7 \times 10^4$, the bin size of the histogram is $\Delta z = 0.5$, the data points are located at the centers of the bins.
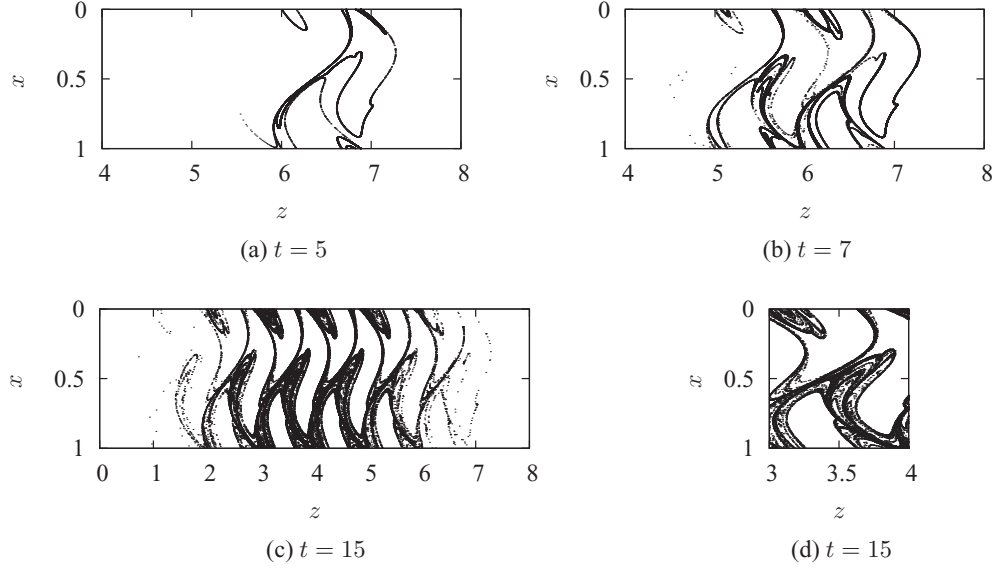
FIG. 3. (a)–(c) Evolution of an ensemble of $N = 62\,500$ particles initially localized in the square $0.2 < x < 0.25$ and $7.75 < z < 7.8$ in the (x,z) plane. Fractal filamentation becomes evident. (d) The pattern of the fourth cell. $W = 0.2$.

that the time evolution of the histogram of the z coordinates precisely follows the Gaussian form

$$n(z,t) = \frac{N\Delta z}{\sqrt{2\pi\sigma(t)^2}} \exp\left\{-\frac{[z - Z(t)]^2}{2\sigma(t)^2}\right\}, \qquad (4)$$

where Δz is the bin size of the histogram.

The diffusional spreading implies a kind of apparently stochastic behavior due to the chaotic dynamics of the individual particles. The existence of the nontrivial terminal fall velocity w can be qualitatively understood by the investigation of the spatial structure of an initially strongly localized ensemble of particles (Fig. 3). Deterministic chaos produces fractal filaments, a nonuniform pattern in space, and this inhomogeneity is the qualitative reason for w to differ from the still fluid settling velocity W. The actual pattern within a single cell is similar to that of the chaotic attractor of the doubly periodic problem (see [3]).

The dependence of the observed settling velocity w on the still fluid settling velocity W and the flow strength B is summarized in Table I. For flow strengths $B = 0.3$ or less, the long-term motion is quasiperiodic. Similarly, a torus can be found for some other parameter values as well, denoted by t in Table I. As we are only interested in chaotic motion, we do not investigate these cases. From Table I one can see that the difference $w - W$ (including its sign) changes irregularly as a

function of B.[1] The diffusion coefficient D is found to exhibit a trend of monotonic growth with B.

B. Transient chaos in finite columns

In the case of a finite column and a long-time observation, chaos will be transient since particles leave the column eventually. Transiently chaotic systems have a characteristic escape rate κ which can be determined as follows. We fill the column with uniformly distributed particles of number N_0 at rest. For each particle (at position $\mathbf{x}$) the escape time $T(\mathbf{x})$ (time needed to leave the column from $\mathbf{x}$) can be determined. The distribution $n(T)$ of the escape times has an exponential tail with exponent κ. This quantity is the escape rate since the integral of $n(T)$ from $T = t$ to infinity gives the number $N(t)$ of the particles still present in the column at time t. Results are shown in Fig. 4 for $M = 8$, and yield an escape rate $\kappa = 0.35$.

Transient chaos is characterized by a chaotic saddle. The saddle and its stable and unstable manifolds can be obtained by means of the sprinkler method (see e.g., [30,31]) that we slightly modified in order to take into account the nonchaotic

---

[1]We have also investigated the limit $A \to \infty$ implying the solution of the equation $\dot{\mathbf{r}} = \mathbf{u}(\mathbf{r},t) - W\mathbf{n}$. The average settling velocity is found to practically coincide with the one describing a resting medium.

TABLE I. The dependence of the difference between the measured settling velocity w and the still fluid settling velocity W on the parameters W and B. t denotes the appearance of a torus. $N \approx 10^4$ for each simulation, $A = 5$.

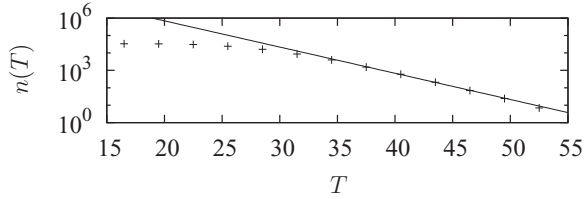| W \ B	0.4	0.5	0.6	0.7	0.8	0.9	1	1.5	2	2.5	5
0.051	0.18	0.08	0.02	−0.05	−0.01	0	−0.02	−0.01	0.03	−0.02	0.02
0.2	0.12	0.08	t	−0.04	−0.03	−0.05	t	−0.07	−0.02	−0.06	0.04
0.5	0.09	0.04	0.05	0.06	−0.01	−0.04	−0.08	t	−0.09	−0.09	0.01

FIG. 4. Histogram of the escape times T of $N_0 \approx 3.2 \times 10^5$ particles, initially distributed homogeneously at rest in a column of height $M = 8$. The escape rate is obtained as $\kappa = 0.35$ from a fit to the interval $T \in [36,48]$. $W = 0.2$. The grid size of the histogram is $\Delta T = 3$.

effect of the uniform settling velocity W in Eq. (2).[2] The results are shown in Fig. 5. The unstable manifold [Fig. 5(c)] of the saddle exhibits the structure of Cantor filaments, the product of a Cantor set and a line. Though the distribution on it strongly depends on height (which is an important feature discussed later), the fractal pattern itself seems to be mostly independent of z. The stable manifold of the chaotic saddle [Fig. 5(a)] is also of Cantor filament type at the bottom, but this structure

_____

[2]The entire column is homogeneously filled with $N_0 \gg 1$ particles at rest, and trajectories spending a time at least $t_0(z)$ within the column are kept. This time is chosen to increase with the initial height z of the particles as $t_0(z) = t_0 + z/W$. The locations of the survived particles at time 0 and $t_0(z)$ provide, for large t_0, a good approximation to the stable and the unstable manifold, respectively, and those at time about $t_0(z)/2$ approximate the saddle.

changes when going upward: a uniformly distributed, space-filling random pattern becomes more and more dominant. A characteristic height dependence can be seen in the chaotic saddle as well. It exhibits the structure of a double Cantor set at the bottom of the column. When going upward, the saddle's shape converges to that of the unstable manifold [as can be seen in Fig. 5(b)]. This is consistent with the fact that any saddle is the intersection of its stable and unstable manifolds [31]. It is worth emphasizing that the dynamics described by Eq. (2) has a four-dimensional phase space. What we see in the fluid is a projection of the phase space objects onto the (x,z) plane. As for the stable manifold of the saddle, the method provides its intersection with the (x,z) plane. Correspondingly, if the particles are initiated with the fluid velocity, the stable manifold appears with a different pattern, while the saddle and its unstable manifold remain unchanged.

The stagger-and-step method [32] provides a way to generate high resolution plots of chaotic saddles. The basic idea is as follows. Let us consider a trajectory composed of discrete (numerical) steps, with $\mathbf{x}_n$ designating the position corresponding to the nth step. For each step, the escape time $T(\mathbf{x}_n)$ (time needed to leave the column from $\mathbf{x}_n$) can be determined. Following the particle along this trajectory (increasing n), $T(\mathbf{x}_n)$ decreases. When it drops below a prescribed value T^*, we look for a nearby point $\mathbf{x}_n + \mathbf{r}_n$ with $T(\mathbf{x}_n + \mathbf{r}_n) > T^*$ [32]. Then we change the position to $\mathbf{x}_n + \mathbf{r}_n$, and continue with a new trajectory. Repeating this algorithm for every occurrence of $T(\mathbf{x}_n) < T^*$ we can assure that the particle never leaves the column. The trajectory obtained this
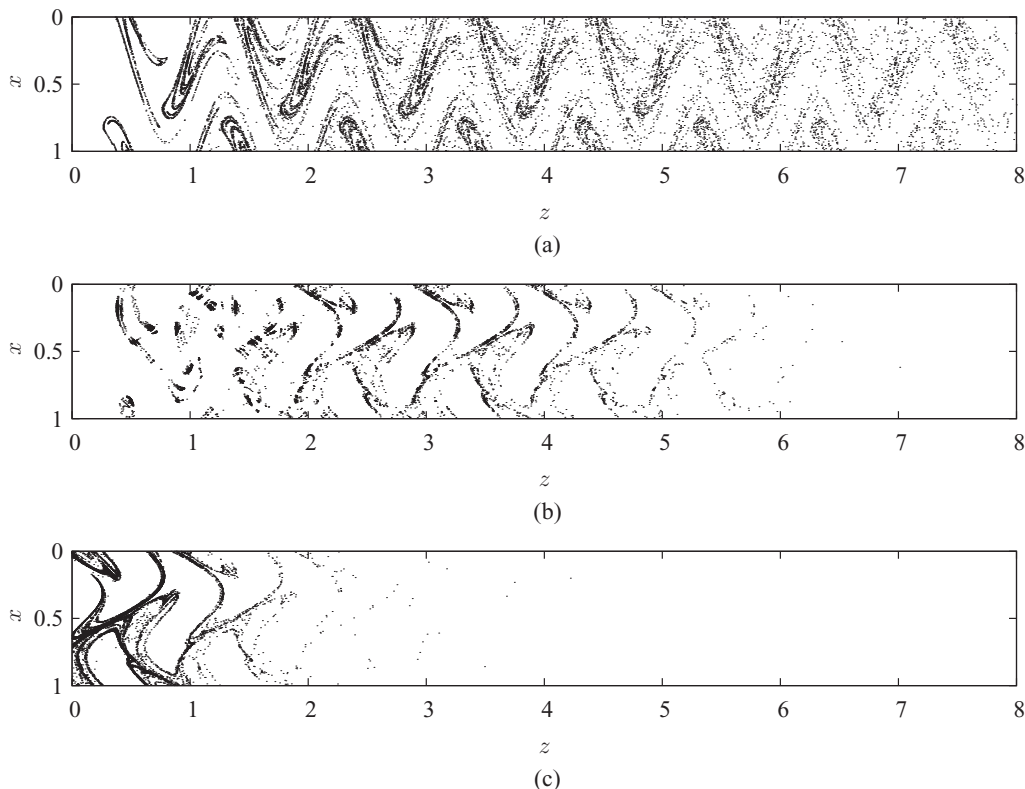

(a)

(b)

(c)

FIG. 5. Spatial structure of the chaotic saddle (b) and its stable (a) and unstable (c) manifold obtained by means of the sprinkler method. $W = 0.2$, $M = 8$, $t_0 = 6$, $N_0 \approx 2 \times 10^6$.
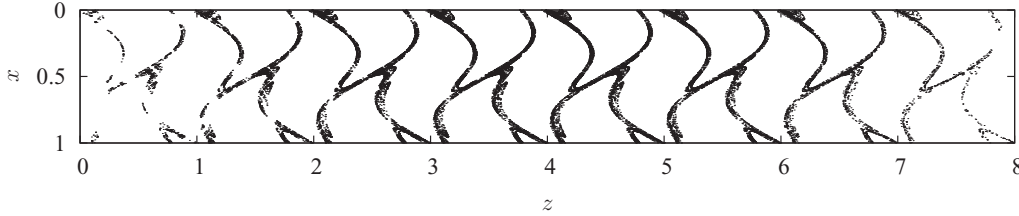
FIG. 6. Spatial structure of the chaotic saddle projected onto the (x,z) plane obtained by means of the stagger-and-step method ($T^* = 30$, $\max(|\mathbf{r}_n|) = 10^{-7}$). $W = 0.051$, $M = 8$.

way can be regarded as a "numerical" trajectory on the saddle with a precision of $\max(|\mathbf{r}_n|)$.

In a gravitational field this method has to be modified for long columns. We define an effective escape time $\tilde{T}$ from which the linear trend of the nonchaotic settling is deduced:

$$\tilde{T}(\mathbf{x}) := T(\mathbf{x}) - z/W, \qquad (5)$$

and replace the escape time $T(\mathbf{x})$ by the effective escape time $\tilde{T}(\mathbf{x})$.

Using the modified stagger-and-step method, we find that a large portion of the long trajectory on the saddle is restricted to the lower part of the column. For the investigation of this property, it is worth considering lower values W of the still fluid settling velocity.

High-resolution results are presented in Fig. 6 for $W = 0.051$. We notice that the double Cantor form is "filled up" again when going upward from the bottom, but it reappears at the top. To quantitatively formulate our observation on the height dependence of the fractal structure, we calculated the box-counting dimension D_0 of a given area in each cell of the saddle. Figure 7 shows that the dimension D_0 of the chaotic saddle is significantly smaller in the lowest and in the uppermost cells than in the middle of the column where it appears to be constant over several cells, in accordance with Fig. 6. Since the dimension for a union of fractals is the maximum of that of the components, the overall fractal dimension of the saddle is given by the dimension far from the boundaries. We mention that location-dependent fractality has also been observed in growing microbial colonies [33].

A qualitative explanation for the height dependence can be given as follows. Points of the chaotic saddle within a single cell of the column can be classified in a hierarchical manner: (i) trajectories never leaving the cell itself and (ii) trajectories never leaving the cell and one of its neighboring cells, etc. In a cell far from the bound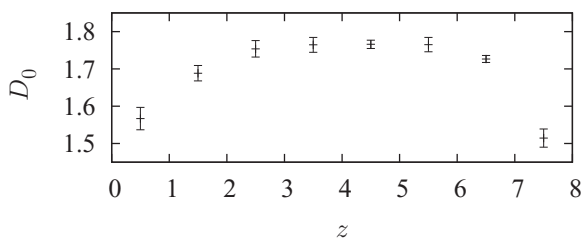aries many levels of this hierarchy are present. Higher levels are however absent in cells that lie closer to a boundary. This causes the saddle to be more sparse near the boundaries. The vertical asymmetry is due to the presence of the gravitational field.

As previously mentioned, the points of a long trajectory on the chaotic saddle are distributed unevenly along the vertical direction on large scales. This property appears in Fig. 6 as a height dependence in the density of the points of the saddle. We now turn to a more detailed investigation of this global distribution. Numerically we create a histogram of the z coordinates of the points of an ensemble of stagger-and-step trajectories initiated at different points. For the histogram we integrate over all velocity components as well as over the horizontal coordinate x. We choose the bin size to be one half of the cell size $\Delta z = 0.5$. The density of points in each bin is denoted by $\rho(z)$, where z is the center of the bin. The density is normalized by assuring its integral over the entire column to be 1. This coarse-grained density on the chaotic saddle is shown in Fig. 8. As expected from Fig. 6 there is a dominant maximum and there are local minima at the boundaries of the column. The results practically do not depend on the parameters T^* and $\max(|\mathbf{r}_n|)$ in the ranges [30,45] and [$10^{-10}, 10^{-7}$], respectively.

In the terminology of dynamical systems, the stationary distribution on the saddle is the natural measure. The one along the unstable manifold, called the conditionally invariant measure, is also of special importance [22,34]. The previous one characterizes the dynamics of particles that never leave the saddle. The conditionally invariant measure, however, describes how particles *deviate* from the chaotic saddle and can be regarded as one maintained by supplying new points into the region of interest according to the rate at which trajectories
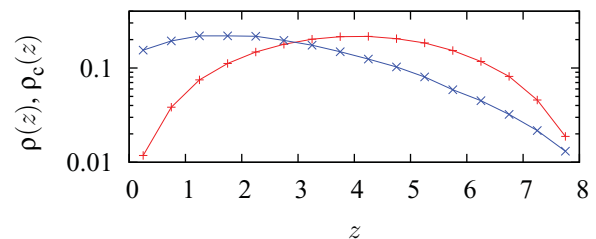

FIG. 7. Box-counting dimension D_0 (with error bars) of the chaotic saddle in Fig. 6 for each cell determined from the region $0.35 < x < 0.7$ and $m + 0.4 < z < m + 0.75$, $m = 0, 1, \ldots, 7$.

FIG. 8. (Color online) Coarse-grained density $\rho(z)$ (" $+$ " marks) of the z coordinates of seven stagger-and-step trajectories of total length of $\approx 2 \times 10^6$ time units on the chaotic saddle [$T^* = 30$, $\max(|\mathbf{r}_n|) = 10^{-7}$], and coarse-grained density $\rho_c(z)$ ("x" marks) of $N \approx 60\,000$ particles along the unstable manifold, approximating the conditionally invariant measure. $W = 0.051$, $M = 8$. The grid size of the histograms is $\Delta z = 0.5$.
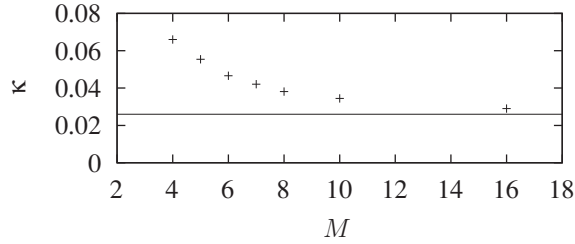
FIG. 9. Escape rate κ as a function of column height M. The number of particles initiated in each column is $N_0 \approx 40\,000M$ for $M \leqslant 15$ ($N_0 \approx 65\,000$ for $M = 16$). The horizontal line indicates the value of κ found for the semi-infinite column, based on a simulation initiated with $N \approx 1.6 \times 10^5$ particles of the conditionally invariant measure. $W = 0.051$.

FIG. 10. (Color online) Semi-infinite column. Coarse-grained density $\rho(z)$ ("+" marks) of the z coordinates of 19 stagger-and-step trajectories of total length of $\approx 7.5 \times 10^5$ time units on the chaotic saddle [$T^* = 45$, $\max(|\mathbf{r}_n|) = 10^{-10}$], and coarse-grained density $\rho_c(z)$ ("x" marks) of $N \approx 1.6 \times 10^5$ particles approximating the conditionally invariant measure. $W = 0.051$. The grid size of the histograms is $\Delta z = 0.5$.

escape from the region asymptotically. This latter measure thus reflects the properties of the transport away from the chaotic saddle, and has been demonstrated to be relevant in several transient-chaos-related phenomena [35,36].

We determine the conditionally invariant measure as follows. Initially we homogeneously fill some part of the column with $N \gg 1$ particles at rest. We let them evolve in time and whenever a particle leaves the column we randomly choose another particle and insert a new particle into a small neighborhood of the chosen particle. If a stationary distribution is obtained this way, it will be the conditionally invariant measure by definition.

For the coarse-grained conditionally invariant distribution we generated the normalized histogram [denoted by $\rho_c(z)$] of the z coordinates of the ensemble of N particles described above. The result is shown in Fig. 8. This coarse-grained density also has a maximum, but it is shifted toward the lower part of the column compared to the natural distribution. Local minima at the boundaries of the column are also found.

These observations indicate that fine fractal distributions in the phase space lead to *smooth*, differentiable densities in the vertical direction z when observed on sufficiently coarse scales.

C. Semi-infinite column

Here we turn to the investigation of a semi-infinite column, that is, we change the boundary conditions: particles going upward are never lost. First of all we are interested in the value of the escape rate κ. The most reliable way of determining it is to let the particles of the conditionally invariant measure leave the column. The number of the particles in the column then exhibits an exponential decay with exponent κ. Our numerical result is $\kappa = 0.026$.[3] In Fig. 9 we can see that the series of the escape rates of finite columns of increasing height M tends to this value.

The results obtained for the coarse-grained natural and conditionally invariant measures of the semi-infinite column are shown in Fig. 10 based on the same methods as for finite
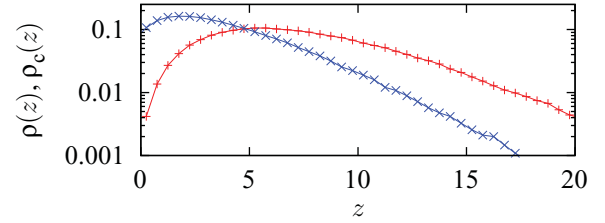
columns. The main shape of the distributions which appear to be smooth remains the same, while their tails are longer. The results on the natural measure are now parameter independent in the ranges $T^* \in [30, 45]$ and $\max(|\mathbf{r}_n|) \in [10^{-10}, 10^{-9}]$.

Having seen the very smooth, regular structure of the coarse-grained density in spatial coordinate z, it is worth investigating the distribution of its conjugated velocity component v_z. Since the velocities are small, any coarse features in space can only be related to the time average of v_z over one period of the driving shear flow, that is over $\Delta t = 1$. In what follows we shall present results for this average velocity, and for the sake of simple notation, we denote this average by v_z as well. Numerically we generated bivariate histograms of the number $n(z, v_z)$ of particles in each bin with variables z and v_z. In Fig. 11(a) we can see the slices taken at fixed values of v_z of the histogram on the saddle. The shape in variable z is nearly independent of the slice taken, that is, the density is close to the product form $n(z, v_z) = f(z)\lambda(v_z)$. As for variable v_z, it is enough then to investigate the histogram $n(v_z)$ integrated over all values of z [shown in Fig. 11(b)]. The density seems to have no regular structure. The strong dependence on the bin size suggests that $n(v_z)$ is not smooth at all.

Turning to the unstable manifold of the saddle, Fig. 12(a) suggests that the product form of the density is not valid, especially at the bottom of the column. The bivariate density in Fig. 12(b) exhibits irregular, nonsmooth behavior in the direction v_z again.

So far we have investigated the system by means of a stroboscopic map, that is, we have taken sections of the phase space at integer time instants. In order to obtain results on the escaping particles, we now take the section of the unstable manifold of the saddle with the plane $z = 0$, but we do not specify the time instant to provide sufficient amount of data. The resulting manifold is shown in three dimensions in Fig. 13. It is remarkable that particles escape only in the interval $x \in [0.7, 1.1]$ and only with horizontal velocities $0 < v_x < 0.2$ as a consequence of the particular form (3) of the flow. The structure seen in Fig. 13 is similar to that of the stroboscopic unstable manifold [for a projection on the (x, z) plane see Fig. 5(c) for $W = 0.2$]. The box counting dimension of the mentioned two-dimensional projection for $W = 0.051$ is found (as described in the caption of Fig. 7) to be $D_0 = 1.75$, which shows a reasonable agreement with $D_0 = 1.73$ of the continuous-time variant of Fig. 13 projected onto the (v_x, v_z)

_____

[3]We must mention that the method generating the conditionally invariant measure is a little bit noisy. Therefore the results presented in this paper are calculated as an average over different realizations.
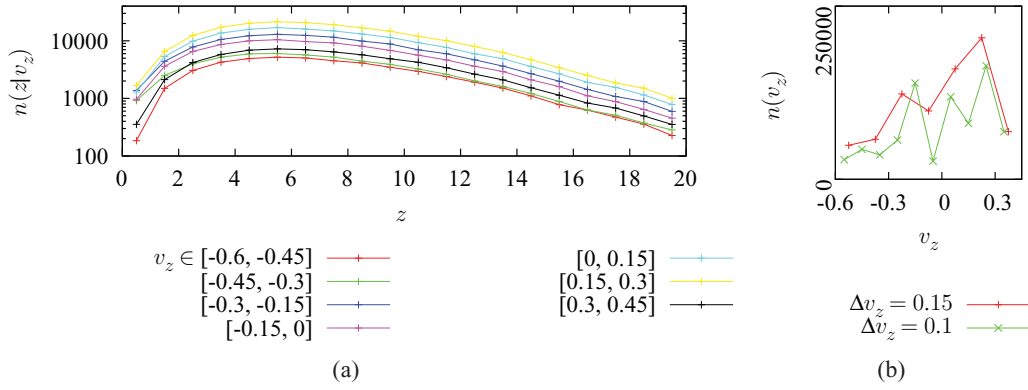
FIG. 11. (Color online) (a) Slices along variable z at fixed intervals of v_z of the bivariate histogram $n(z, v_z)$ of the natural measure based on 19 stagger-and-step trajectories of total length of $\approx 7.5 \times 10^5$ time units on the chaotic saddle $[T^* = 45, \max(|\mathbf{r}_n|) = 10^{-10}]$. The grid size of the histogram is $\Delta z = 1$. (b) One-dimensional histograms of v_z for two bin sizes. $W = 0.051$.

plane. This is in accordance with the fact that we investigate different projections of the same five-dimensional manifold.

IV. A STOCHASTIC APPROACH

In order to find an explanation for the coarse-grained version of the conditionally invariant measure of the semi-infinite column, we consider the effect of the velocity field **u** as a kind of random influence, and investigate the Fokker–Planck equation [37] for a drifting Brownian particle in the vertical direction. In a hydrodynamical context this approach has recently been applied to obtain a stationary probability density for swimming microorganisms in turbulent velocity fields [38]. Here we extend it to an open case. We have seen that the coarse-grained distribution is nonsmooth in variable v_z. Because of this, and since the dimensionless relaxation rate is large, it appears to be reasonable to take the strong friction limit. The dimensionless Fokker–Planck equation then takes the form

$$\frac{\partial P(z,t)}{\partial t} = w^* \frac{\partial P(z,t)}{\partial z} + D^* \frac{\partial^2 P(z,t)}{\partial z^2}, \tag{6}$$

where $P(z,t)$ is the probability density of the particle to be at height z at time t. The values of the drift $-w^*$ and the diffusion coefficient D^* characterizing the conditionally invariant measure of the semi-infinite column are yet unknown. Equation (6) can also be interpreted as an advection-diffusion equation.

The time-dependent distribution of particles along the unstable manifold exhibits a long-term exponential decay with the escape rate κ. This leads to the conclusion that the coarse-grained conditionally invariant density can be identified with the first eigenfunction of the Fokker–Planck equation, with eigenvalue $\exp(-\kappa)$. Substituting $P(z,t) \sim e^{-\kappa t} P(z)$ and prescribing boundary conditions $P(z = 0) = 0$ (as particles are lost there) and $\lim_{z\to\infty} P(z) = 0$, we find the first eigenfunction to be

$$P(z) = \frac{1}{1/\alpha_- - 1/\alpha_+} (e^{-\alpha_- z} - e^{-\alpha_+ z}), \tag{7}$$

where

$$\alpha_\pm = \frac{w^*}{2D^*} \pm \sqrt{\left(\frac{w^*}{2D^*}\right)^2 - \frac{\kappa}{D^*}}. \tag{8}$$

The value of κ is known from our simulations (see Sec. III C). In Sec. III A we have seen that the chaotic effect of the velocity field **u** can modify the settling velocity from W (the drift in still fluid) to a nontrivial one and can lead to the appearance of a well-defined diffusion coefficient. For the conditionally invariant measure of the semi-infinite column, a self-consistent method can be worked out for the determination of w^* and D^*.

With probability density (7) we can calculate the mean values of z-dependent quantities. The vertical velocity v_z is,
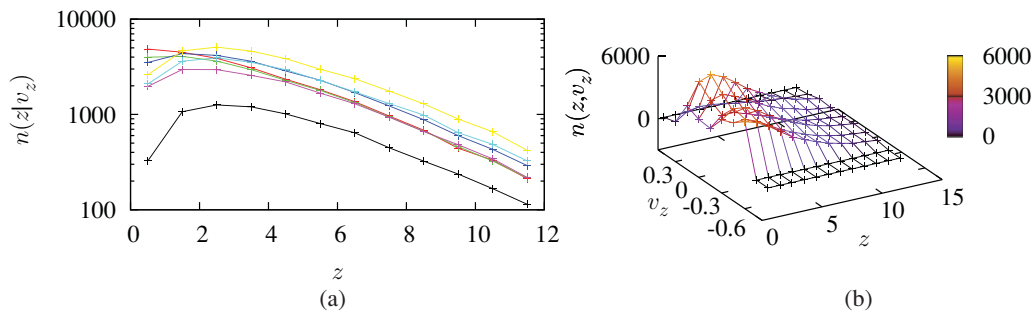

FIG. 12. (Color online) (a) Same as Fig. 11(a) for $N \approx 1.6 \times 10^5$ points approximating the conditionally invariant measure. (b) Bivariate histogram $n(z, v_z)$ in the same simulation. The coloring corresponds to the values on the third axis. The grid sizes of the histogram are $\Delta z = 1$ and $\Delta v_z = 0.15$. $W = 0.051$.
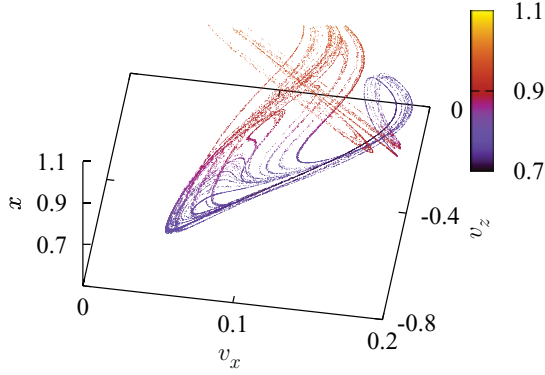
FIG. 13. (Color online) Section of the continuous-time unstable manifold of the saddle with the plane $z = 0$. The coloring corresponds to the x coordinate. The number of the particles applied in the simulation is $N \approx 5 \times 10^4$. $W = 0.051$.

however, not a variable of the strong friction limit Fokker–Planck equation. It can be read off from the relation $J(z,t) = v_z P(z,t)$, where $J(z,t) = -w^* P(z,t) - D^* \partial P(z,t)/\partial z$ is the probability current determined by Eq. (6). Since $P(z,t)$ is the first eigenfunction, we can also write $J(z,t) = e^{-\kappa t} J(z)$. For the probability density (7) the probability current turns out to be

$$J(z) = \frac{w^*}{2(1/\alpha_- - 1/\alpha_+)} \left\{ -\left[1 + \sqrt{1 - \frac{4D^* \kappa}{(w^*)^2}} \right] e^{-\alpha_- z} \right.$$
$$\left. + \left[1 - \sqrt{1 - \frac{4D^* \kappa}{(w^*)^2}} \right] e^{-\alpha_+ z} \right\}, \quad (9)$$

from which $v_z = J(z)/P(z)$.

Evaluating averages with the steady state probability density $P(z)$ (maintained by repumping particles) we obtain analytically that

$$\langle v_z \rangle \equiv \int_0^\infty v_z P(z)\,dz = -w^*, \quad (10)$$

and similarly, one can check that

$$D^* = \langle z v_z \rangle - \langle z \rangle \langle v_z \rangle. \quad (11)$$

We can now calculate these quantities over our numerical approximation to the conditionally invariant measure. We use again the time averaged version of the particle coordinate v_z with $\Delta t = 1$, and for consistency we also use a similar time averaged version of the particle coordinate z as well. The numerical results for the drift and the diffusion coefficient are $w^* = 0.106$ and $D^* = 0.08$. Note that these values differ from $w = 0.130$ and $D = 0.17$ of an infinite column (see Sec III A) since they characterize a situation where the particle distribution strongly overlaps with the bottom of the column.

If our assumptions are correct, function (7) with these numerically obtained parameters (and κ) will have to match our numerical result on the coarse-grained version of the conditionally invariant measure. Figure 14 shows a good agreement.

In view of this, we can say that the two distributions coincide:
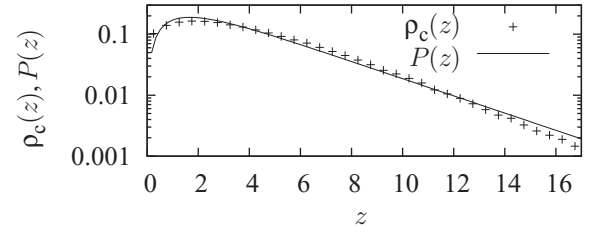
$$P(z) = \rho_c(z), \quad (12)$$

FIG. 14. Normalized coarse-grained histogram $\rho_c(z)$ of the particles of the numerical approximation to the conditionally invariant measure [same as in Fig. 10 with time averaged z coordinates] and the first eigenfunction $P(z)$ [see (7)] of the Fokker–Planck equation with parameters obtained from the same simulation.

the first eigenfunction of (6) is the coarse-grained density of the conditionally invariant measure. The results above imply

$$w^* = -\langle v_z \rangle_c \quad (13)$$

and

$$D^* = \langle z v_z \rangle_c - \langle z \rangle_c \langle v_z \rangle_c, \quad (14)$$

that is, the averages are taken with respect to the conditionally invariant measure. Equation (13) suggests that whether w^* is larger or smaller than W (see Table I) depends on the particular form of this measure. Note that expression (14) is a kind of Green–Kubo formula [39].

It is worth mentioning that the Gaussian

$$P(z,t) = \frac{1}{\sqrt{2\pi\sigma(t)^2}} \exp\left[-\frac{(z + wt)^2}{2\sigma(t)^2} \right] \quad (15)$$

with $\sigma(t)^2 = 2Dt$ is a solution of the strong friction limit Fokker–Planck equation (6) with the initial condition of a Dirac δ centered at $z = 0$, with no boundary conditions, and using $w^* = w$ and $D^* = D$. These choices correspond to an infinite column. Apart from the offsets Z_0 and σ_0^2, function (15) is the one observed in the settling dynamics (Sec. III A, Fig. 2).

We might try to explain the coarse-grained distribution observed on the chaotic saddle as well. On this invariant set we should observe the stationary distribution of Fokker–Planck equation (6), which is a single exponential in variable z. The distribution in Fig. 10 is different. This break-down of the Fokker–Planck method indicates that the natural measure of the saddle, even if coarse grained, cannot be described by an advection-diffusion equation since there is no macroscopic transport associated with the chaotic saddle.

V. CONCLUSIONS

One of the main conclusions of this study is that chaotic saddles in spatially extended systems might have, on the one hand, a local fractality depending on the spatial coordinate along which the extension is large. On the other hand, in spite of the intricate fractal patterns in the phase space, smooth coarse-grained densities might be found in this spatial coordinate. Such coarse-grained densities can then be described by macroscopic equations like the Fokker–Planck or the advection-diffusion equation. In open systems, the conditionally invariant density is of special importance since

it describes the transport away from the chaotic set. Its coarse-grained version was shown to be the first nontrivial eigenfunction of the Fokker–Planck equation.

Another important feature of our problem is the existence of a drift velocity due to the presence of the gravitational field. A numerical observation is that the measured settling velocity in the flow differs from the one appearing in a still fluid.

We have also found that the drift velocity and the diffusion coefficient appearing in the Fokker–Planck equation describing the conditionally invariant measure of a semi-infinite column should be different from the ones observed for long-term settling in an infinite column. This may be a consequence of the different spatial structures characterizing these two cases. The conditionally invariant measure, for example, exhibits a special height dependence due to the absorbing boundary condition at the bottom [see Fig. 5(c)]. The role of the underlying structure is well illustrated by the fact that the average vertical velocity taken with respect to the natural measure turns out to be zero, numerically. It indicates again that the chaotic saddle itself cannot be associated with any macroscopic transport.

In general, we can conclude that macroscopic transport properties are influenced by the chaotic behavior of the particles. The difference between the settling velocity in the presence of a flow and that in a still fluid, the dependence of the fractal dimension on height, the presence of a nontrivial local maximum in the coarse grained densities, the applicability of a Fokker–Planck model to an open chaotic system, and the observation that transport coefficients are to be interpreted as averages taken with respect to the conditionally invariant measure, might be relevant in the dynamics of rain droplets, of volcanic ash particles, in demixing experiments, and other related phenomena.

[1] J. Bec, Phys. Fluids **15**, L81 (2003).

[2] Y. Do and Y.-C. Lai, Phys. Rev. Lett. **91**, 224101 (2003).

[3] R. D. Vilela, T. Tél, A. P. S. de Moura, and C. Grebogi, Phys. Rev. E **75**, 065203(R) (2007).

[4] R. D. Vilela and A. E. Motter, Phys. Rev. Lett. **99**, 264101 (2007).

[5] J. C. Zahnow and U. Feudel, Phys. Rev. E **77**, 026215 (2008).

[6] J. C. Zahnow, R. D. Vilela, U. Feudel, and T. Tél, Phys. Rev. E **77**, 055301(R) (2008); **80**, 026311 (2009).

[7] F. Toschi and E. Bodenschatz, Annu. Rev. Fluid. Mech. **41**, 375 (2009).

[8] J. H. E. Cartwright, U. Feudel, Gy. Károlyi, A. de Moura, O. Piro, and T. Tél, in *Nonlinear Dynamics and Chaos: Advances and Perspectives*, edited by M. Thiel, J. Kurths, M. C. Romano, Gy. Károlyi, and A. de Moura (Springer, Berlin, 2010).

[9] R. A. Shaw, Ann. Rev. Fluid Mech. **35**, 183 (2003).

[10] G. Falkovich and A. Pumir, J. Atm. Sci. **64**, 4497 (2007).

[11] A. Jaczewski and S. P. Malinowski, Q. J. R. Meteorol. Soc. **131**, 2047 (2005).

[12] A. Fouxon, M. G. Stepanov, and G. Falkovich, Nature (London) **419**, 151 (2002).

[13] A. L. Alldredge, T. Granata, C. Gotschalk, and T. Dickey, Limnol. Oceanogr. **35**, 1415 (1990).

[14] T. Kiorboe and G. A. Jackson, Limnol. Oceanogr **46**, 1309 (2001).

[15] M. Lunau, A. Lemke, O. Dellwig, and M. Simon, Limnol. Oceanogr. **51**, 847 (2006).

[16] H. R. Pruppacher and J. D. Klett, *Microphysics of Clouds and Precipitation* (Kluwer Academic, Dordrecht, The Netherlands, 1997).

[17] F. H. Ludlam, *Clouds and Storms* (The Pennsylvania State University Press, University Park, 1980).

[18] A. Flentje *et al.*, Atmos. Chem. Phys. **10**, 10085 (2010).

[19] J. Vollmer, G. K. Auernhammer, and D. Vollmer, Phys. Rev. Lett. **98**, 115701 (2007).

[20] J. Vollmer, J. Chem. Phys. **129**, 1 (2008).

[21] I. J. Benczik and J. Vollmer, Eur. Phys. Lett. **91**, 360003 (2010).

[22] T. Tél, in *Directions in Chaos, 3*, edited by B.-L. Hao (World Scientific, Singapore, 1990), p. 149.

[23] J. R. Dorfman, *From Molecular Chaos to Dynamical Chaos* (Cambridge University Press, Cambridge, 1999).

[24] P. Gaspard, *Chaos, Scattering and Statistical Mechanics* (Cambridge University Press, Cambridge, 1999).

[25] J. Vollmer, T. Tél, and W. Breymann, Physica D **187**, 108 (2004); J. Vollmer, Phys. Rep. **372**, 131 (2002).

[26] M. R. Maxey and J. J. Riley, Phys. Fluids **26**, 883 (1983).

[27] T. R. Auton, J. Hunt, and M. Prud'homme, J. Fluid. Mech. **197**, 241 (1988).

[28] M. Liu, F. Muzzio, and R. Peskin, Chaos Sol. Fract. **4**, 869 (1994).

[29] R. T. Pierrehumbert, Chaos Sol. Fract. **4**, 1091 (1994).

[30] E. Ott, *Chaos in Dynamical Systems*, 2nd ed. (Cambridge University Press, Cambridge, 2002).

[31] T. Tél and M. Gruiz, *Chaotic Dynamics* (Cambridge University Press, Cambridge, 2006).

[32] D. Sweet, H. E. Nusse, and J. A. Yorke, Phys. Rev. Lett. **86**, 2261 (2001).

[33] G. Károlyi, Phys. Rev. E **71**, 031915 (2005).

[34] G. Pianigiani and J. A. Yorke, Trans. Amer. Math. Soc. **252**, 351 (1979).

[35] E. G. Altmann and T. Tél, Phys. Rev. Lett. **100**, 174101 (2008).

[36] E. G. Altmann, Phys. Rev. A **79**, 013830 (2009).

[37] L. E. Reichl, *A Modern Course in Statistical Physics* (Wiley-VCH, Weinheim, Germany, 2009).

[38] C. Torney and Z. Neufeld, Phys. Rev. Lett. **101**, 078105 (2008).

[39] J. R. Dorfman, *An Introduction to Chaos in Nonequilibrium Statistical Mechanics* (Cambridge University Press, Cambridge, 1999).